ACS MATERIALS LETTERS

www.acsmaterialsletters.org

Influence of Pressure, Particle Morphology, Coating, and Heat Treatment on the Effective Electronic Conductivity of Cathode Active Materials for All-Solid-State Batteries

Vanessa Miß, Stefan Seus, Anna Marx, Elisa D. Steyer, Valeriu Mereacre, Joachim R. Binder, and Bernhard Roling*

Cite This: ACS Materials Lett. 2025, 7, 2262−2269

ABSTRACT: For modeling electrochemical processes in all-solid-state batteries, reliable values for the electronic conductivity of cathode active materials (CAM) are of the utmost importance. Published values for a specific CAM vary by typically many orders of magnitude. Therefore, we carried out a systematic study on the influence of various experimental parameters on the effective electronic conductivity of CAM pellets. These parameters are applied stack pressure, Ni content of CAM, CAM particle morphology, particle coating, and heat treatment. Pellets of fully lithiated and uncoated Ni-rich NMC particles reach effective electronic conductivities σ_{eon}^{eff} in the range of 10^{-1} S/cm at high pressures and 10^{-2} S/cm at low pressures. Particle coating by $LiNbO_3$ lowers σ_{eon}^{eff} by half an order to 1 order of magnitude. While heat treatment at 900 °C is capable of removing surface impurities on the CAM particle, it also leads to increased Li/Ni disorder in the bulk of the particles.

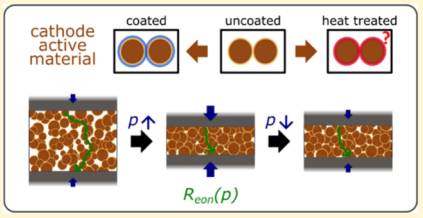

Lithium-ion batteries are important devices for mobile as well as for stationary energy storage.[1,2] State-of-the-art batteries reach energy densities in the range of 250 Wh/kg,[3] thus approaching their physicochemical limit. Higher energy densities can potentially be achieved in bulk-type all-solid-state lithium batteries (ASSBs) by using metallic lithium as negative electrode material.[4] The positive electrode of such an ASSB is a composite consisting of active material particles (CAM = cathode active material), solid electrolyte (SE) particles, and, if necessary, electronically conductive additives, like carbon black.[5,6] A classical CAM is $LiCoO_2$ (LCO), which in the last two decades has been replaced, to a large extent, by Ni-rich $LiNi_xMn_yCo_zO_2$ (NMC) with $x + y + z = 1$.[7−9] Since many SEs, in particular sulfide-based SEs, are oxidized in direct contact to LCO and NMC, the CAM particles are often coated by a thin ion-conductive layer, e.g. a $LiNbO_3$ or a $LiTaO_3$ layer.[10−14]

In ASSBs, the pressure plays an important role for establishing good contacts between the particles. Consequently, accurate values for the ionic conductivity of SE particles and the electronic conductivity of CAM particles at different pressures are of utmost importance for modeling electrochemical processes in ASSBs.[15−18] While the ionic conductivity of many SEs was measured with rather high accuracy,[19,20] experimental studies on the electronic conductivity of CAMs are scarce, and values reported for the electronic conductivity of a specific CAM vary often by several orders of magnitude. For instance, studies on fully lithiated LCO yielded room-temperature electronic conductivities in the range of 10^{-8} S/cm − 10^{-3} S/cm.[21,22] While in the case of Menetrier et al.,[21] the LCO particles were heat-treated at 900 °C for 36 h with intermediate grinding, Wang et al. applied spark plasma sintering at 800 °C.[22] Heat treatment seems to exert also a strong influence on the electronic conductivity of fully lithiated NMC. After a heat treatment in the range of 850 °C − 1000 °C, either on a particle level for $x = 0.33$[23] or on a pellet level for $x = 0.33$ and $x = 0.5$,[24,25] electronic conductivities in the range of 10^{-8} S/cm − 10^{-6} S/cm were found. In contrast, higher electronic conductivities were measured for untreated, fully lithiated NMC pellets. Although all studies report an increase in electronic conductivity with an increase in Ni content, there are huge discrepancies in the reported values: Asano et al. and Siroma et al. obtained values of $7{\cdot}10^{-5}$ S/cm at $x = 0.33$[26] and 10^{-3} S/cm at $x = 0.5$,[27]

Received: December 20, 2024
Revised: April 29, 2025
Accepted: May 12, 2025
Published: May 16, 2025

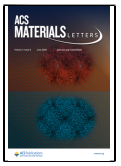

https://doi.org/10.1021/acsmaterialslett.4c02595
ACS Materials Lett. 2025, 7, 2262−2269

respectively. On the other hand, Wang et al.[22] reported an electronic conductivity of spark-plasma sintered NMC particles, increasing with the Ni content from $2{\cdot}10^{-6}$ S/cm at $x = 0.3$ to $2{\cdot}10^{-2}$ S/cm at $x = 0.8$. Here the question arises as to whether the electronic conductivity variations at similar or even identical chemical compositions are mainly due to different heat treatments or whether other experimental parameters, such as coating of the particles and stack pressure during the measurements, also play an important role for the electronic conductivity. Overall, the existing literature values do not allow for clearly deciphering the influence of different experimental parameters on the electronic conductivity of CAMs.

Consequently, we have carried out a systematic study on the influence of the following parameters on the effective electronic conductivity of pellets of fully lithiated LCO particles and NMC particles, respectively: (i) stack pressure during measurement; (ii) Ni content of NMC; (iii) particle morphology; (iv) coating of the particles with a thin $LiNbO_3$ layer using two different techniques; and (v) heat treatment of the particles. To this end, impedance spectra of CAM pellets sandwiched between metal electrodes were taken and analyzed. The results give strong indication for high bulk electronic conductivities of Ni-rich NMC particles already in the fully lithiated state. We note that this study is a first step toward a better understanding of the pressure-dependent properties of composite electrodes in a second step and of the pressure-dependent properties of complete ASSBs in a third step.

All sample preparations were carried out in a glovebox (UniLab, MBraun, Garching, Germany) under an argon atmosphere with $x_{H2O} < 1$ ppm and $x_{O2} < 1$ ppm.

Single-crystalline $LiCoO_2$ (LCO) was purchased as uncoated particles from Alfa Aesar (Karlsruhe, Germany) and as $LiNbO_3$-coated particles (average coating thickness of 12 nm) from Toda (Japan), respectively. $LiNi_{0.6}Mn_{0.2}Co_{0.2}O_2$ (NMC622) and $LiNi_{0.83}Mn_{0.06}Co_{0.11}O_2$ (NMC83611) were purchased as uncoated polycrystalline and as uncoated single-crystalline particles, respectively, from MSE Supplies (Tucson, USA).

A fraction of the NMC622 particles were coated by 0.5 wt % $LiNbO_3$ by using two different methods, namely a classical sol−gel method and a chemically activated coating process using H_2O_2 as activating agent.[28,29] The chemically activated process typically leads to denser coatings with a more homogeneous thickness. In both cases, the coated particles were heat-treated at 350 °C. The heat treatment of the coated NMC622 particles leads to amorphous or nanocrystalline $LiNbO_3$ layers, while a treatment at higher temperatures leads to microcrystalline $LiNbO_3$ layers with lower Li^+ ion conductivity.[30]

Furthermore, a fraction of the uncoated NMC622 was subjected to a heat treatment under argon atmosphere. To this end, 2 g of sc-NMC622 was placed in an aluminum oxide combustion boat and transferred under an argon atmosphere into a quartz glass tube, which was fixed in a tube furnace (Nabertherm, Lilienthal, Germany). The glass tube was continuously flushed with argon. The particles in the glass tube were heated to 900 °C with a heating rate of 24.5 K/min, held at 900 °C for different holding times, and cooled to RT without control of the cooling rate. Thus, during the heat treatment, the sc-NMC622 particles were constantly kept under an Ar atmosphere without any contact to air.

An overview of all CAM particles used for this study, including their coating and their heat treatment, is given in Table 1.

Table 1. List of All Polycrystalline and Single-Crystalline CAM Particles Used for This Study Including Their Coating and Heat Treatment

Acronym	pc/sc	Coating material	Coating method	Heat treatment temperature and holding time
LCO	sc	x	x	x
LCO	sc	$LiNbO_3$	unknown	x
NMC83611	sc	x	x	x
NMC622	sc	x	x	x
NMC622	sc	$LiNbO_3$	classical sol−gel	x
NMC622	sc	$LiNbO_3$	chem. activation using H_2O_2	x
NMC622	pc	x	x	x
NMC622	pc	$LiNbO_3$	classical sol−gel	x
NMC622	pc	$LiNbO_3$	chem. activation using H_2O_2	x
NMC622	sc	x	x	900 °C for 6 h
NMC622	sc	x	x	900 °C for 12 h
NMC622	sc	x	x	900 °C for 24 h

Two different types of impedance spectra were observed, depending on the electronic resistance R_{eon} of the CAM particles, see Figure 1. In the case of very low resistances in the range of some Ω, the electronic resistance was detected at low frequencies, while a nonideal inductive impedance was observed at high frequencies, see Figure 1 (a). The inductive impedance is caused by the inductance of the cables connecting the sample cells to the NEISYS instrument. The spectra were fitted with a serial $CPE{-}R_{eon}$ equivalent circuit shown in the inset, with the CPE impedance $Z = \frac{1}{Q(i\omega)^{\alpha}}$ with $\alpha > -1$ caused by a nonideal inductance. In the case of high electronic resistances in the range of some 100 Ω, a high-frequency resistance R_1 and a semicircle at low frequencies with diameter R_2 was detected, see Figure 1 (b). The equivalent circuit for fitting is shown in the inset. Since the impedance spectra were measured under ion-blocking conditions, the electronic resistance R_{eon} is identical to the sum $R_1 + R_2$. Hence, the effective electronic conductivity of the CAM pellet is given by $\sigma_{eon}^{eff} = R_{eon}^{-1} \cdot (d/A)$ with d and A denoting the thickness and the area of the pellet. The semicircle was attributed to interfacial impedances between the CAM particles, since the capacitance C_2 obtained from fitting the semicircle was in the range of $10^{-9} - 10^{-8}$ F/cm^2, which is 2−3 orders of magnitude higher than the bulk capacitance of the CAM particles. The ratio of interfacial capacitance to bulk capacitance should be given by the ratio of the coating/impurity layer thickness to the CAM particle diameter, which is indeed in the range $10^2 - 10^3$. The semicircle is only then detectable in the sub-MHz regime, if the time constant $\tau_2 = R_2C_2$ is $>10^{-6}$ s. This implies that R_2 should be >100 Ωcm^2. In this case, the effective electronic conductivity $\sigma_{eon}^{eff} \approx d/R_2$ (d = pellet thickness) $< 10^{-3}$ S/cm. Consequently, all data points with $\sigma_{eon}^{eff} < 10^{-3}$ S/cm are based on spectra as shown in Figure

https://doi.org/10.1021/acsmaterialslett.4c02595
ACS Materials Lett. 2025, 7, 2262−2269

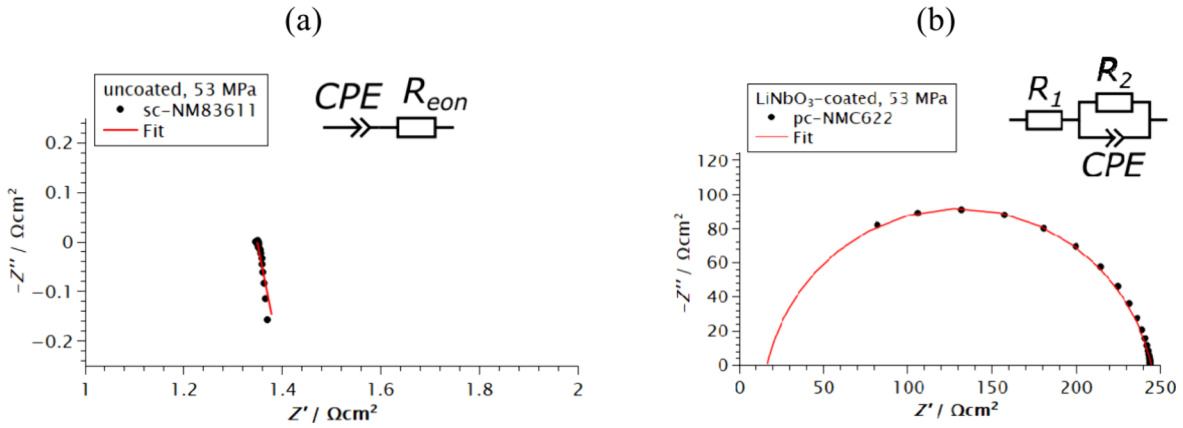

Figure 1. Impedance spectra of (a) uncoated sc-NMC83611 and (b) $LiNbO_3$-coated pc-NMC622 (chemical activation method using H_2O_2) taken at a pressure of 53 MPa and in a frequency range from 1 MHz to 0.1 Hz. The red lines are fits to the equivalent circuits shown in the insets.

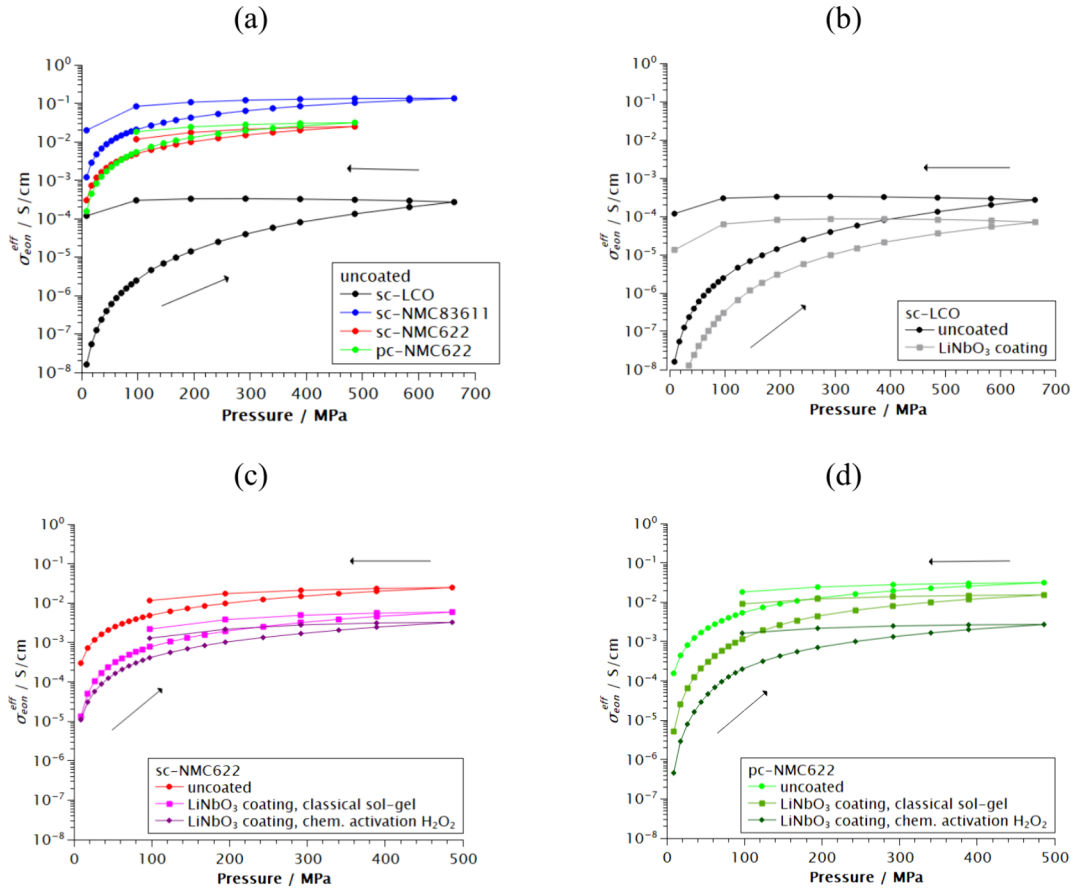

Figure 2. Pressure-dependent effective electronic conductivity σ_{eon}^{eff} of (a) uncoated LCO, sc-NMC622, pc-NMC622, and sc-NMC83611, (b) LCO uncoated and LCO coated with $LiNbO_3$, (c) sc-NMC622 uncoated and coated with $LiNbO_3$ by two different coating techniques, and (d) pc-NMC622 uncoated and coated with $LiNbO_3$ by two different coating techniques.

1 (b), while data points with $\sigma_{eon}^{eff} > 10^{-3}$ S/cm are based on spectra as shown in Figure 1 (a).

In Figure 2 (a), we plot the effective conductivity σ_{eon}^{eff} of different uncoated and nonheat-treated CAM particles versus the applied stack pressure during the impedance measurement. All CAMs exhibit a similar pressure dependence of σ_{eon}^{eff}. When increasing the pressure up to several 100 MPa, a strong increase of the electronic conductivity by several orders of magnitude is observed. During a subsequent release of the pressure to values of 100 MPa, the effective conductivity remains virtually constant. Only at pressures below 100 MPa does a slight conductivity drop takes place. This gives strong indication that the applied pressure of several 100 MPa leads to an irreversible densification of the sample pellets and, in turn, an improved contact between the CAM particles. When the pressure is released, the particle contacts stay intact; however, below 100 MPa, the particle contacts start to worsen.

https://doi.org/10.1021/acsmaterialslett.4c02595
ACS Materials Lett. 2025, 7, 2262−2269

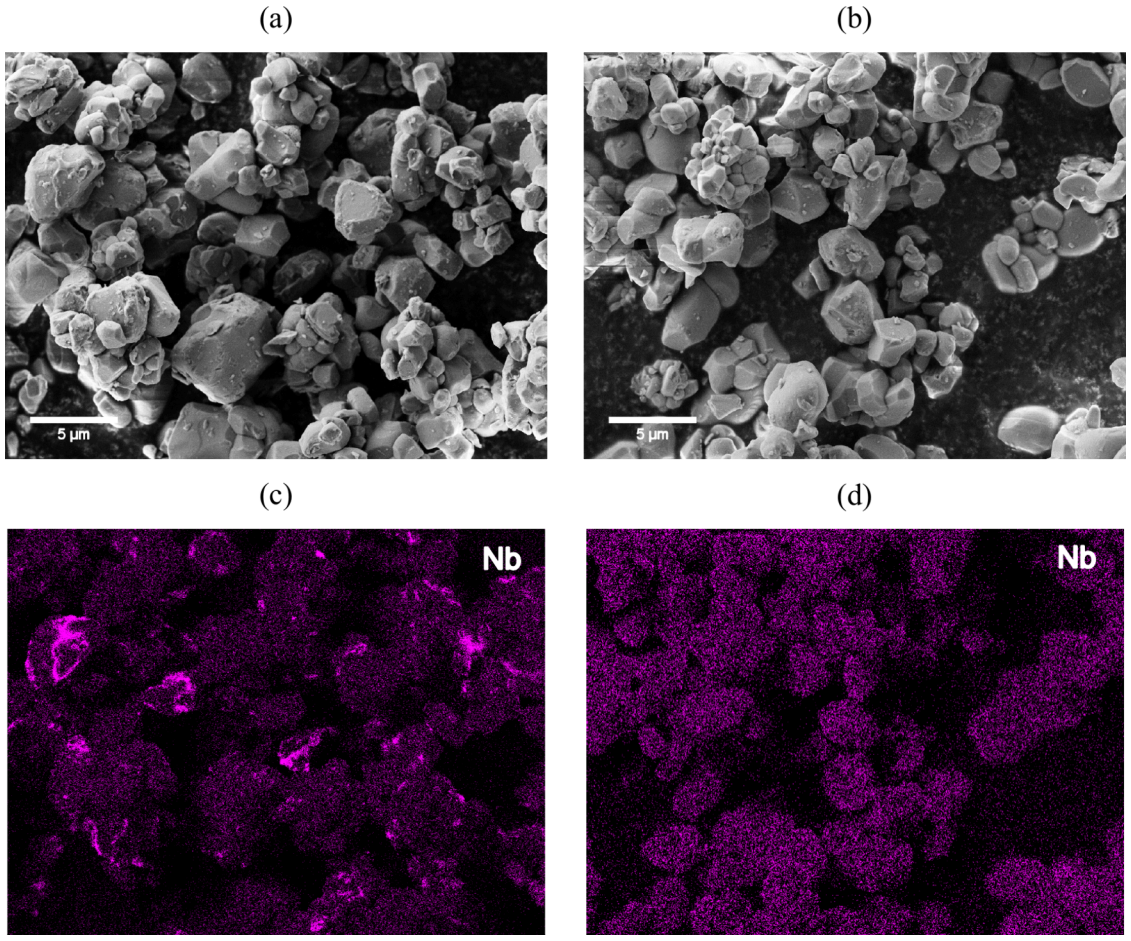

Figure 3. SEM images of sc-NMC622 particles with (a) $LiNbO_3$ coating by a classical sol−gel method and (b) $LiNbO_3$ coating by a chemically activated process using H_2O_2. Nb-EDX element mappings of sc-NMC622 particles with (c) $LiNbO_3$ coating by a classical sol−gel method and (d) $LiNbO_3$ coating by a chemically activated process using H_2O_2.

This suggests that the applied pressure does not lead to pressure-induced sintering of the CAM particles.

When comparing the effective conductivity of different uncoated CAM at high pressures (Figure 2 (a)), the following trends are observed: (i) The electronic conductivity increases with the Ni content (LCO: $1.3{\cdot}10^{-4}$ S/cm; sc-NMC622: $2.5{\cdot}10^{-2}$ S/cm; sc-NMC83611: 10^{-1} S/cm at 486 MPa). This is in accordance with the literature.[22,26,27] (ii) pc-NMC622 ($3.1{\cdot}10^{-2}$ S/cm) exhibits a slightly higher electronic conductivity than sc-NMC622 ($2.5{\cdot}10^{-2}$ S/cm) at 486 MPa.

A closer look at the pressure dependence of σ_{eon}^{eff} for pc-NMC622 and sc-NMC622 reveals an intersection of the curves around 75 MPa. Below 75 MPa, the electronic conductivity of sc-NMC622 is higher, but the electronic conductivity of pc-NMC622 increases more strongly with pressure. This suggests that in pc-NMC622, the existence of the nanoscale primary particles inside the secondary particles leads to a stronger irreversible densification of the pellets. In addition, SEM images of the pellet surfaces and of cross-sectional cuts into the pellets by a focused ion beam are shown in Figure S2 and S3 and reveal that pressure leads indeed to a stronger irreversible densification of the pc-NMC pellets. An increasing pressure causes cracking of secondary particles and a subsequent change of the secondary particle morphology. These morphological changes enable denser packing of the secondary particles. In the case of the sc-NMC622 pellets, there is exclusively a decrease in the void space between the sc particles and no deformation of the sc particles.

In Figure 2 (b), we compare the pressure-dependent effective electronic conductivity of uncoated and $LiNbO_3$-coated sc-LCO. As shown in Figure S4 in the Supporting Information, the $LiNbO_3$ coating is dense and homogeneous. The pressure dependence of σ_{eon}^{eff} is similar for both CAM pellets; however, the coating lowers the absolute values of σ_{eon}^{eff} by about 1 order of magnitude. In Figure 2 (c) and (d), pressure-dependent σ_{eon}^{eff} data are plotted for uncoated and $LiNbO_3$-coated sc-NMC622 and for uncoated and $LiNbO_3$-coated pc-NMC622, respectively. As shown in the SEM/EDX images in Figure 3, the classical sol−gel method leads to an inhomogeneous coating of the sc-NMC622 particles, whereas the chemically activated process using H_2O_2 as activating agent leads to a dense and homogeneous coating. The same can be observed for pc-NMC622, see SEM/EDX images in Figure S5 in the Supporting Information. As seen from Figure 2 (c) and (d), the classical sol−gel coating lowers σ_{eon}^{eff} by about half an order of magnitude, while the chemically activated coating lowers σ_{eon}^{eff} by about 1 order of magnitude. The lowering of σ_{eon}^{eff} may be due to either the electronic resistance of the coating itself or a reduction of the electronic contact area between the particles by the coating.

In Figure 4 (a), we show the effect of heat treatments on the effective electronic conductivity of uncoated sc-NMC622. The

https://doi.org/10.1021/acsmaterialslett.4c02595
ACS Materials Lett. 2025, 7, 2262−2269

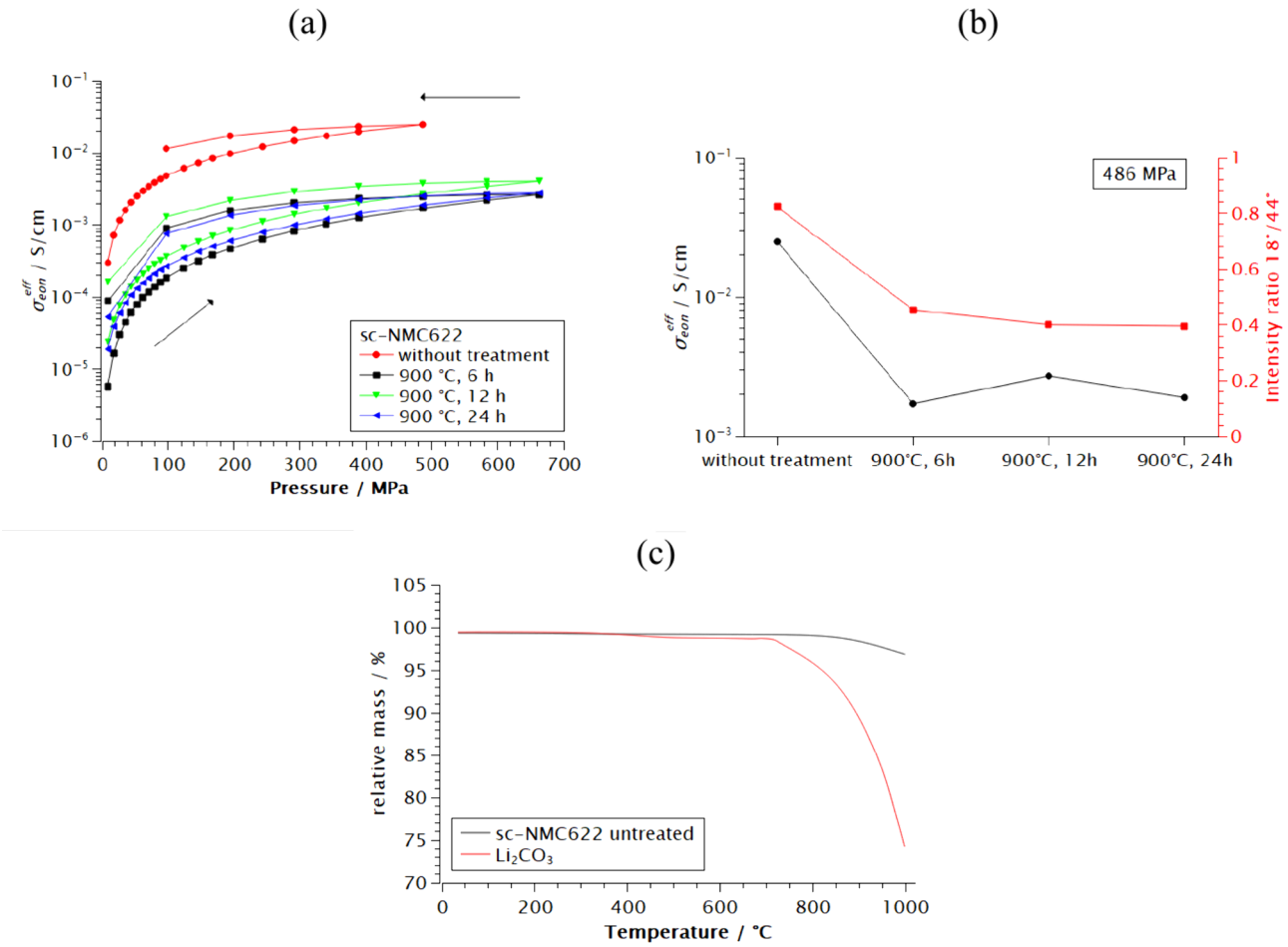

Figure 4. (a) **Influence of heat treatment on the pressure-dependent effective electronic conductivity σ_{eon}^{eff} of sc-NMC622; (b) σ_{eon}^{eff} at 486 MPa and intensity ratio of the Bragg peaks at 18° and 44° of sc-NMC622 plotted versus the holding time at 900 °C (XRD pattern of sc-NMC622 in SI, Figure S6); (c) thermogravimetric analysis of untreated sc-NMC622 and pure Li_2CO_3.**

heat treatment was carried out at 900 °C under an Ar atmosphere for different periods of time (holding times). We note that 900 °C is in the typical range of heat treatment temperatures applied in the literature.[23−25] A short heat treatment with a holding time of 6 h leads to a drop of the effective electronic conductivity at high pressures by about 1 order of magnitude. For longer holding times of 12 and 24 h, the effective electronic conductivity is higher than after 6 h holding time. In Figure 4 (b), the influence of the holding time at 900 °C on the electronic conductivity is plotted for a pressure of 486 MPa, revealing a minimum effective electronic conductivity after 6 h of holding time. The existence of this minimum suggests the influence of two opposing factors on the effective electronic conductivity.

In Figure 4 (b), we show the influence of the heat treatment time on the intensity ratio of the two NMC622 Bragg peaks, namely, at 18° and at 44°. This ratio is a measure for the Li/Ni ordering inside the NMC particles.[31,32] The complete XRD patterns of sc-NMC622 at different holding times are shown in Figure S6 in the Supporting Information. After 6 h of holding time, the intensity ratio drops significantly, indicating increased Li/Ni disorder. Longer holding times do not change the intensity ratio and thus the Li/Ni disorder significantly. This increased disorder is most likely responsible for a drop of the bulk electronic conductivity after a 6 h holding time.

In Figure 5, we show SEM images of the uncoated sc-NMC622 particles after different heat treatments. For untreated sc-NMC622, the particles exhibit an irregular shape with a strongly varying diameter. After a holding time of 6 h, coral-like structures appear on the particle surface, which disappear again after 12 and 24 h of holding time. We suggest that this phenomenon is related to Li_2CO_3, which is a well-known impurity on the surface of NMC particles.[32−34] As shown in Figure 4 (c), thermogravimetric analysis (TGA) of untreated sc-NMC622 particles and of pure Li_2CO_3 reveals a mass loss above 800 °C due to decomposition of Li_2CO_3 into Li_2O and CO_2. The relative mass of pure Li_2CO_3 is expected to drop from 100% to about 40% (ratio M_{Li2O}/M_{Li2CO3}) at high temperatures, while the relative mass drop of NMC with only a small amount of Li_2CO_3 impurities is much lower. According to Figure 4 (c), it seems likely that after 6 h of holding time, the Li_2CO_3 layer has partially decomposed into Li_2O, and that a demixing of Li_2CO_3 and Li_2O leads to the coral-like structure. After 12 and 24 h holding time, the carbonate layer is completely decomposed, and thus, the coral-like structure has disappeared. Instead, Li_2O impurity particles appeared between the CAM particles. This is supported by the SEM/EDX images shown in Figure 5 (e,f), respectively, for 24 h holding time. The EDX element mappings of uncoated sc-NMC622 and the heat-treated CAM for 6 and 12 h are shown in Figure S7 in the Supporting Information. The newly

https://doi.org/10.1021/acsmaterialslett.4c02595
ACS Materials Lett. 2025, 7, 2262−2269

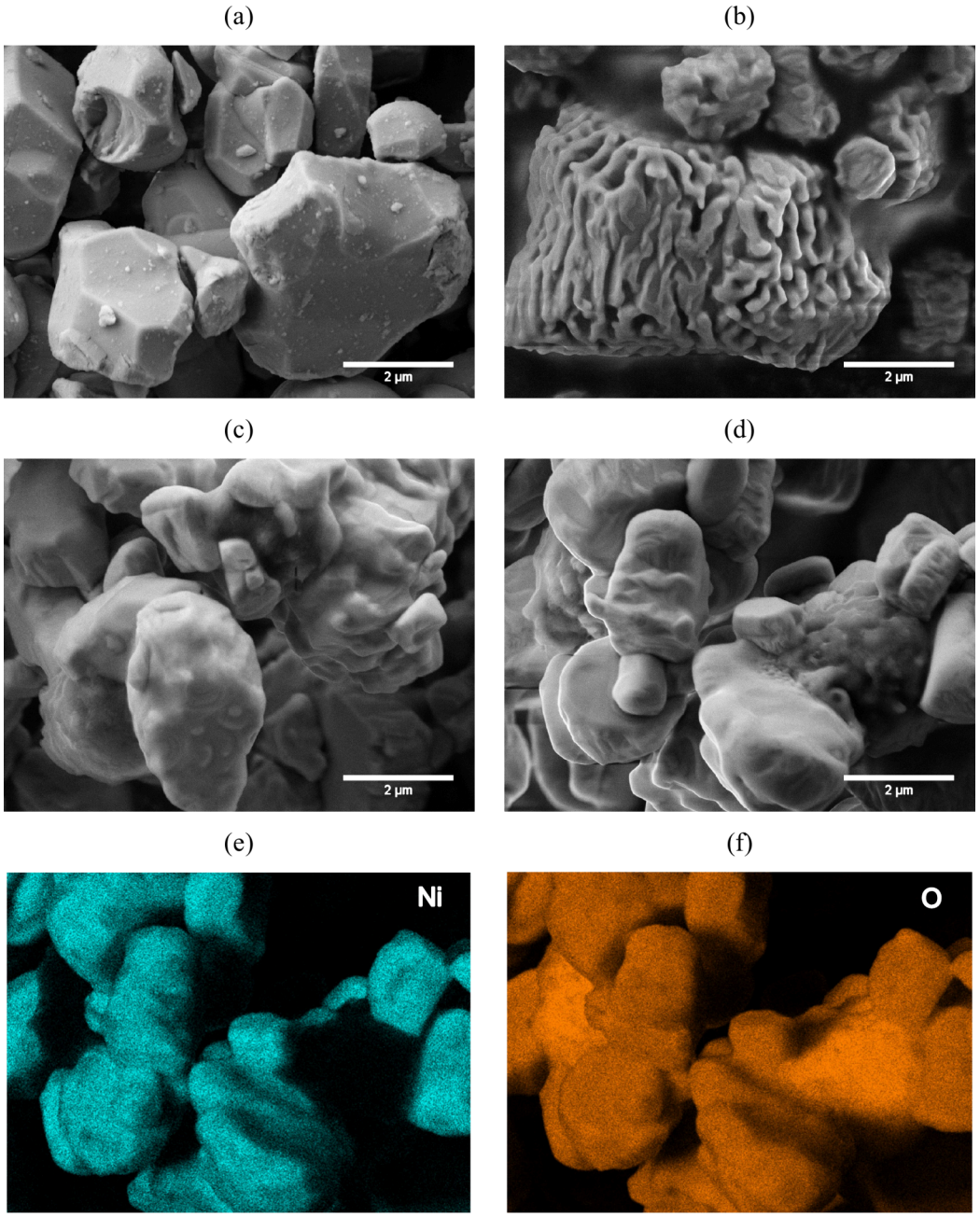

Figure 5. SEM image of the cathode active material sc-NMC622 (a) without any treatment as well as heat-treated at (b) 900 °C for 6 h, (c) 900 °C for 12 h, and (d) 900 °C for 24 h. EDX element mappings of sc-NMC622 particles heat-treated at 900 °C for 24 h for (e) nickel and (f) oxygen.

appeared particles exhibit a different shape as the CAM particles, and an oxygen signal is the only detectable EDX signal on these particles. These observations give strong indication that the coral-like structures on the CAM particles after 6 h of holding time hinder the interparticle electron transport, while the Li_2O impurity particles between the NMC particles do not significantly hinder electron transport. Furthermore, an EDX spectrum of all elements in the impurity particles between the CAM particles is shown in Figure S8 in the Supporting Information. No Ni EDX signal is detected, and only a very tiny carbon signal is detected. The carbon signal is too small to arise from Li_2CO_3 but originates most likely from the carbon pad below the particles. Therefore, we can clearly exclude that the impurity particles are composed of Li_2CO_3. Overall, the opposing influence of surface impurity on the CAM particles and of the bulk Li/Ni disorder on the effective electronic conductivity leads to a minimum of σ_{eon}^{eff} after a holding time of 6 h. Since the increase in Li/Ni disorder due to heat treatment is a bulk effect, this effect is also expected to take place in pc-NMC particles. This explains the low electronic conductivities reported for pc-NMC with x = 0.33.[23]

In conclusion, our results give new insights into the origin of the highly differing values published in the literature for the effective electronic conductivity of CAM particles. In order to achieve high σ_{eon}^{eff} values close to the bulk electronic conductivity of the CAM particles, the particles have to be densified by applying pressures of several 100 MPa. Thereafter,

https://doi.org/10.1021/acsmaterialslett.4c02595
ACS Materials Lett. 2025, 7, 2262−2269

the pressure can be released to about 100 MPa without a significant drop in the effective electronic conductivity. However, below 100 MPa, the effective conductivity drops by a factor of 2−3 indicating a worsening of the particle−particle contacts. At low pressures, sc-NMC particles exhibit higher σ_{con}^{eff} values than pc-NMC particles, while the opposite effect is observed at high pressures. Furthermore, a high Ni content is advantageous for the electronic conductivity of the NMC.

Coating layers on the CAM particles, as well as bulk Li/Ni disordering in the CAM, lower the effective electronic conductivity of a CAM pellet. Without $LiNbO_3$ coating, σ_{con}^{eff} values in the range of 10^{-1} S/cm at high pressures and 10^{-2} S/cm at low pressures are achievable, despite the existence of Li_2CO_3 impurities on the CAM particle surfaces. Although Li_2CO_3 can be decomposed by a heat treatment, this heat treatment leads to Li/Ni disordering in the bulk of the CAM particles and does therefore *not* improve the effective electronic conductivity. A dense and homogeneous $LiNbO_3$ coating is important for suppressing decomposition of the solid electrolyte by the CAM particles in the composite cathodes of all-solid-state batteries. However, as shown in this study, such a coating reduces σ_{con}^{eff} to values in the range of 10^{-3} S/cm at low pressures.

■ ASSOCIATED CONTENT

Supporting Information

The Supporting Information is available free of charge at https://pubs.acs.org/doi/10.1021/acsmaterialslett.4c02595.

Experimental methods; SEM images of pc-NMC622 and sc-NMC622 pellet surfaces; cross-sectional SEM images after an FIB cut of pc-NMC622 pellets and sc-NMC622 pellets; SEM/EDX images of $LiNbO_3$-coated LCO particles; cross-sectional image of $LiNbO_3$-coated LCO particles inside a composite cathode; SEM images of $LiNbO_3$-coated pc-NMC622 particles; XRD patterns of untreated and heat-treated sc-NMC622 particles; EDX element mappings of untreated and heat-treated sc-NMC622 particles; SEM/EDX data of heat-treated sc-NMC622 particles (PDF)

■ AUTHOR INFORMATION

Corresponding Author

Bernhard Roling − *Department of Chemistry, Philipps-Universität Marburg, D-35032 Marburg, Germany;* orcid.org/0000-0001-7383-1495; Email: roling@staff.uni-marburg.de

Authors

Vanessa Miß − *Department of Chemistry, Philipps-Universität Marburg, D-35032 Marburg, Germany*

Stefan Seus − *Department of Chemistry, Philipps-Universität Marburg, D-35032 Marburg, Germany*

Anna Marx − *Department of Chemistry, Philipps-Universität Marburg, D-35032 Marburg, Germany*

Elisa D. Steyer − *Department of Chemistry, Philipps-Universität Marburg, D-35032 Marburg, Germany*

Valeriu Mereacre − *Karlsruhe Institute of Technology (KIT), Institute for Applied Materials (IAM-ESS), D-76344 Eggenstein-Leopoldshafen, Germany;* orcid.org/0000-0002-8295-6078

Joachim R. Binder − *Karlsruhe Institute of Technology (KIT), Institute for Applied Materials (IAM-ESS), D-76344 Eggenstein-Leopoldshafen, Germany;* orcid.org/0000-0003-2237-1411

Complete contact information is available at: https://pubs.acs.org/10.1021/acsmaterialslett.4c02595

Author Contributions

CRediT: **Vanessa Miß** conceptualization, formal analysis, investigation, visualization, writing - original draft, writing - review & editing; **Stefan Seus** formal analysis, investigation; **Anna Marx** formal analysis, investigation; **Elisa D. Steyer** formal analysis, investigation; **Valeriu Mereacre** resources, writing - review & editing; **Joachim R. Binder** resources, writing - review & editing; **Bernhard Roling** conceptualization, funding acquisition, resources, supervision, writing - original draft, writing - review & editing.

Notes

The authors declare no competing financial interest.

■ ACKNOWLEDGMENTS

We are grateful to the German Science Foundation (DFG) for financial support of this work (Grant No. Ro1213/20-1).

■ REFERENCES

(1) Gandoman, F. H.; Jaguemont, J.; Goutam, S.; Gopalakrishnan, R.; Firouz, Y.; Kalogiannis, T.; Omar, N.; Van Mierlo, J. Concept of Reliability and Safety Assessment of Lithium-Ion Batteries in Electric Vehicles: Basics, Progress, and Challenges. *Appl. Energy* **2019**, *251*, 113343.

(2) Whittingham, M. S. Lithium Batteries: 50 Years of Advances to Address the Next 20 Years of Climate Issues. *Nano Lett.* **2020**, *20*, 8435−8437.

(3) Hirsh, H. S.; Li, Y.; Tan, D. H. S.; Zhang, M.; Zhao, E.; Meng, Y. S. Sodium-Ion Batteries Paving the Way for Grid Energy Storage. *Adv. Energy Mater.* **2020**, *10*, 2001274.

(4) Janek, J.; Zeier, W. G. A Solid Future for Battery Development. *Nat. Energy* **2016**, *1*, 16141.

(5) Dong, S.; Sheng, L.; Wang, L.; Liang, J.; Zhang, H.; Chen, Z.; Xu, H.; He, X. Challenges and Prospects of All-Solid-State Electrodes for Solid-State Lithium Batteries. *Adv. Funct. Mater.* **2023**, *33*, 2304371.

(6) Zeng, Z.; Cheng, J.; Li, Y.; Zhang, H.; Li, D.; Liu, H.; Ji, F.; Sun, Q.; Ci, L. Composite Cathode for All-Solid-State Lithium Batteries: Progress and Perspective. *Mater. Today Phys.* **2023**, *32*, 101009.

(7) de Biasi, L.; Schwarz, B.; Brezesinski, T.; Hartmann, P.; Janek, J.; Ehrenberg, H. Chemical, Structural, and Electronic Aspects of Formation and Degradation Behavior on Different Length Scales of Ni-Rich NCM and Li-Rich HE-NCM Cathode Materials in Li-Ion Batteries. *Adv. Mater.* **2019**, *31*, 1900985.

(8) Jamil, S.; Wang, G.; Fasehullah, M.; Xu, M. Challenges and Prospects of Nickel-Rich Layered Oxide Cathode Material. *J. Alloys Compd.* **2022**, *909*, 164727.

(9) Li, H.; Wang, L.; Song, Y.; Zhang, Z.; Du, A.; Tang, Y.; Wang, J.; He, X. Why the Synthesis Affects Performance of Layered Transition Metal Oxide Cathode Materials for Li-Ion Batteries. *Adv. Mater.* **2024**, *36*, 2312292.

(10) Hu, G.; Tao, Y.; Lu, Y.; Fan, J.; Li, L.; Xia, J.; Huang, Y.; Zhang, Z.; Su, H.; Cao, Y. Enhanced Electrochemical Properties of $LiNi_{0.8}Co_{0.1}Mn_{0.1}O_2$ Cathode Materials Modified with Lithium-Ion Conductive Coating $LiNbO_3$. *ChemElectroChem.* **2019**, *6*, 4773−4780.

(11) Chen, H.; Deng, Z.; Li, Y.; Canepa, P. On the Active Components in Crystalline Li-Nb-O and Li-Ta-O Coatings from First Principles. *Chem. Mater.* **2023**, *35*, 5657−5670.

(12) Bong, W. S. K.; Shiota, A.; Miwa, T.; Morino, Y.; Kanada, S.; Kawamoto, K. Effect of Thickness and Uniformity of $LiNbO_3$-Coated Layer on $LiNi_{0.5}Co_{0.2}Mn_{0.3}O_2$ Cathode Material on Enhancement of Cycle Performance of Full-Cell Sulfide-Based All-Solid-State Batteries. *J. Power Sources* **2023**, *577*, 233259.
(13) Hu, X.; Zhao, Z.; Zhao, Y.; Wang, X.; Sainio, S.; Nordlund, D.; Ruse, C. M.; Zhou, X. D.; Boettcher, S. W.; Hou, D.; et al. Interfacial Degradation of the NMC/Li_6PS_5Cl Composite Cathode in All-Solid-State Batteries. *J. Mater. Chem. A* **2024**, *12*, 3700−3710.
(14) Wu, J.; Shen, L.; Zhang, Z.; Liu, G.; Wang, Z.; Zhou, D.; Wan, H.; Xu, X.; Yao, X. All-Solid-State Lithium Batteries with Sulfide Electrolytes and Oxide Cathodes. *Electrochem. Energy Rev.* **2021**, *4*, 101−135.
(15) Xu, H.; Yu, Y.; Wang, Z.; Shao, G. First Principle Material Genome Approach for All Solid-State Batteries. *Energy Environ. Mater.* **2019**, *2*, 234−250.
(16) Bielefeld, A.; Weber, D. A.; Janek, J. Modeling Effective Ionic Conductivity and Binder Influence in Composite Cathodes for All-Solid-State Batteries. *ACS Appl. Mater. Interfaces* **2020**, *12*, 12821−12833.
(17) Yildiz, E.; Serpelloni, M.; Salvadori, A.; Cabras, L. A Comparative Review of Models for All-Solid-State Li-Ion Batteries. *Batteries* **2024**, *10*, 150.
(18) Vadhva, P.; Hu, J.; Johnson, M. J.; Stocker, R.; Braglia, M.; Brett, D. J. L.; Rettie, A. J. E. Electrochemical Impedance Spectroscopy for All-Solid-State Batteries: Theory, Methods and Future Outlook. *ChemElectroChem.* **2021**, *8*, 1930−1947.
(19) Ohno, S.; Bernges, T.; Buchheim, J.; Duchardt, M.; Hatz, A. K.; Kraft, M. A.; Kwak, H.; Santhosha, A. L.; Liu, Z.; Minafra, N.; et al. How Certain Are the Reported Ionic Conductivities of Thiophosphate-Based Solid Electrolytes? An Interlaboratory Study. *ACS Energy Lett.* **2020**, *5*, 910−915.
(20) Cronau, M.; Szabo, M.; König, C.; Wassermann, T. B.; Roling, B. The Stack Pressure Dilemma OfHow to Measure a Reliable Ionic Conductivity? The Stack Pressure Dilemma of Microcrystalline Sulfide-Based Solid Electrolytes. *ACS Energy Lett.* **2021**, *6*, 3072−3077.
(21) Ménétrier, M.; Saadoune, I.; Levasseur, S.; Delmas, C. The Insulator − Metal Transition upon Lithium Deintercalation from $LiCoO_2$: Electronic Properties and ^{7}Li NMR Study. *J. Mater. Chem.* **1999**, *9*, 1135−1140.
(22) Wang, S.; Yan, M.; Li, Y.; Vinado, C.; Yang, J. Separating Electronic and Ionic Conductivity in Mix-Conducting Layered Lithium Transition-Metal Oxides. *J. Power Sources* **2018**, *393*, 75−82.
(23) Burkhardt, S.; Friedrich, M. S.; Eckhardt, J. K.; Wagner, A. C.; Bohn, N.; Binder, J. R.; Chen, L.; Elm, M. T.; Janek, J.; Klar, P. J. Charge Transport in Single NCM Cathode Active Material Particles for Lithium-Ion Batteries Studied under Well-Defined Contact Conditions. *ACS Energy Lett.* **2019**, *4*, 2117−2123.
(24) Amin, R.; Chiang, Y.-M. Characterization of Electronic and Ionic Transport in $Li_{1-x}Ni_{0.33}Mn_{0.33}Co_{0.33}O_2$ (NMC333) and $Li_{1-x}Ni_{0.50}Mn_{0.20}Co_{0.30}O_2$ (NMC523) as a Function of Li Content. *J. Electrochem. Soc.* **2016**, *163*, A1512−A1517.
(25) Zahnow, J.; Bernges, T.; Wagner, A.; Bohn, N.; Binder, J. R.; Zeier, W. G.; Elm, M. T.; Janek, J. Impedance Analysis of NCM Cathode Materials: Electronic and Ionic Partial Conductivities and the Influence of Microstructure. *ACS Appl. Energy Mater.* **2021**, *4*, 1335−1345.
(26) Asano, T.; Yubuchi, S.; Sakuda, A.; Hayashi, A.; Tatsumisago, M. Electronic and Ionic Conductivities of $LiNi_{1/3}Mn_{1/3}Co_{1/3}O_2$-$Li_3PS_4$ Positive Composite Electrodes for All-Solid-State Lithium Batteries. *J. Electrochem. Soc.* **2017**, *164*, A3960−A3963.
(27) Siroma, Z.; Sato, T.; Takeuchi, T.; Nagai, R.; Ota, A.; Ioroi, T. AC Impedance Analysis of Ionic and Electronic Conductivities in Electrode Mixture Layers for an All-Solid-State Lithium-Ion Battery. *J. Power Sources* **2016**, *316*, 215−223.
(28) Mereacre, V.; Binder, J. R. Strong-Acid-Catalyzed Formation of Crystalline $LiNbO_3$ at Low Ambient Temperatures. *Inorg. Chem.* **2022**, *61*, 7222−7225.
(29) Mereacre, V.; Stüble, P.; Ghamlouche, A.; Binder, J. R. Enhancing the Stability of $LiNi_{0.5}Mn_{1.5}O_4$ by Coating with $LiNbO_3$ Solid-State Electrolyte: Novel Chemically Activated Coating Process versus Sol-Gel Method. *Nanomaterials* **2021**, *11*, 548.
(30) Heitjans, P.; Masoud, M.; Feldhoff, A.; Wilkening, M. NMR and Impedance Studies of Nanocrystalline and Amorphous Ion Conductors: Lithium Niobate as a Model System. *Faraday Discuss.* **2007**, *134*, 67−82.
(31) Zhao, J.; Zhang, W.; Huq, A.; Misture, S. T.; Zhang, B.; Guo, S.; Wu, L.; Zhu, Y.; Chen, Z.; Amine, K.; et al. In Situ Probing and Synthetic Control of Cationic Ordering in Ni-Rich Layered Oxide Cathodes. *Adv. Energy Mater.* **2017**, *7*, 1601266.
(32) Chen, S.; Zhang, X.; Xia, M.; Wei, K.; Zhang, L.; Zhang, X.; Cui, Y.; Shu, J. Issues and Challenges of Layered Lithium Nickel Cobalt Manganese Oxides for Lithium-Ion Batteries. *J. Electroanal. Chem.* **2021**, *895*, 115412.
(33) Renfrew, S. E.; Kaufman, L. A.; McCloskey, B. D. Altering Surface Contaminants and Defects Influences the First-Cycle Outgassing and Irreversible Transformations of $LiNi_{0.6}Mn_{0.2}Co_{0.2}O_2$. *ACS Appl. Mater. Interfaces* **2019**, *11*, 34913−34921.
(34) Renfrew, S. E.; McCloskey, B. D. Quantification of Surface Oxygen Depletion and Solid Carbonate Evolution on the First Cycle of $LiNi_{0.6}Mn_{0.2}Co_{0.2}O_2$ Electrodes. *ACS Appl. Energy Mater.* **2019**, *2*, 3762−3772.

https://doi.org/10.1021/acsmaterialslett.4c02595
ACS Materials Lett. 2025, 7, 2262−2269